Modeling Mechanical Properties of Knitted Fabric Composites – Part III: Applications

Zheng-Ming Huang
Department of Engineering Mechanics, Tongji University,
1239 Siping Road, Shanghai 200092, P.R. China
E-mail: huangzm@mail.tongji.edu.cn

S. Ramakrishna
Biomaterials Laboratory, Division of Bioengineering
Department of Mechanical Engineering
National University of Singapore, 10 Kent Ridge Crescent,
Singapore 119260

ABSTRACT

This is the last part of a series of papers, presenting the review and summary of a systematically theoretical investigation on the mechanical properties of knitted fabric reinforced laminae (single layer) and laminates (multilayer). The geometric identification for various knitted fabric structures and the theoretical development of the modeling procedure have been described in detail in the previous two papers. The most significant advantage of this modeling is that the composite properties at any loading condition can be determined in terms of those of the constituent fiber and matrix materials which are easily obtainable. The present paper summarizes the results of applications to a number of typical knitted fabric reinforced composites, including thermoset and elastomer matrix based composite laminae and multilayer knitted fabric laminates with different lay-up arrangement. The predicted stiffness, ultimate strength, rubber-elastic relationship, and progressive failure behavior are compared favorably with experimental data. Investigations of the fabric stitching parameters, fiber content, constituent properties, and laminate lay-up patterns on the influence of the composite mechanical behavior are presented. Future trend of simulation on knitted fabric composites is also addressed in the paper.

Key words: Knitted fabric composite, polymer matrix composite, multilayer laminate, mechanical property, stiffness, strength, rubber-elastic behavior, modeling, parametric study

1. INTRODUCTION

In recent years, the present authors and their co-workers have carried out a systematic investigation on the structure-property relationships of various knitted fabric reinforced composites. The theoretical investigation thus made is believed to have merits for the composite community. For the greater benefit of readers, we choose to review and summarize our work in this series of papers.

In the previous two papers /1,2/, the geometric description for different knitted fabric structures and the theoretical development of the modeling procedure have been illustrated. Application examples are addressed in the present paper. These examples are classified into three types, i.e. thermoset matrix based composites, elastomer matrix based composites, and multilayer laminated composites. Three kinds of fabric structures, i.e. plain weft knit, Milano rib knit, and interlock knit have been used as reinforcement.

Regarding the applications of the theoretical modeling, two issues are important. One is simplicity

and the other is accuracy. The simplicity is related to the preparation of input data required for the modeling. In this work, only two kinds of input data are required. They are the properties of the constituent fiber and matrix materials and the composite geometric parameters. While preparing the composite geometric parameters, the most complicated work is to specify the yarn orientation of the reinforcing fabric structure. This kind of work has been described in detail in Ref. /1/. In the present paper, illustration on preparing the constituent properties and the remaining geometric parameters including the fiber volume content, the laminate lay-up angles, and the laminate thickness is shown. These remaining geometric parameters are either simply measured (e.g. through a combustion to obtain the fiber content) or taken from the *in situ* fabrication condition (e.g. the laminate information). The constituent properties are obtained through measurement of the monolithic fiber and matrix specimens, as demonstrated in the paper.

All the application examples have been accompanied with experimental data. These data are also summarized in the paper for comparison. Parametric studies are presented to show the influence of various fabric geometric parameters and different constituent properties on the mechanical behavior of the resulting composites. These results are useful for a composite design.

2. THERMOSET MATRIX COMPOSITES

In this section, analysis results of weft knitted fabric reinforced thermoset matrix composites are presented. Of these matrices, epoxy and polyester resins are the ones mostly used. In this work, all the matrices used are epoxy resins. Two types of knitted fabric composites are considered. One is of plain knitted fabric composites and another is of Milano rib knitted fabric composites. Both fabrics are manufactured using E glass fiber yarns, but the matrices used are somewhat different. Details are described below.

2.1 Plain Knitted Fabric Composites

Plain weft knitted fabric is the most common fabric form. The epoxy-based composites with this kind of fabric reinforcement have been investigated by a number of researchers /3-8/. The following presentation is mainly based on the results of Refs. /5/ and /6/.

2.1.1 Stiffness Simulation

Glass fibers and epoxy resin, both of which are isotropic, with properties of E^f=74GPa, ν^f=0.23, E^m=3.6GPa and ν^m=0.35 respectively, have been used to fabricate the knitted fabric composite. Reference /4/ reported experimentally measured data of this composite, which are summarized in Table 1. Knitted

Table 1

Elastic Properties of Plain Knitted Glass Fiber Fabric Reinforced Epoxy Composites. The parameters used are: E^f=74GPa, ν^f=0.23, E^m=3.6GPa,ν^m=0.35,d=0.0445cm, D_y=177.8, K=0.45, ρ_f=2.54 g/cm^3, C=2.5 cycle/cm, and W=2 cycle/cm.

Model	E_{xx} (GPa)	E_{yy} (GPa)	E_{zz} (GPa)	G_{xy} (GPa)	G_{xz} (GPa)	G_{yz} (GPa)	ν_{xy}	ν_{xz}	ν_{yz}
Exper. /4/	5.38 (0.33)$^{\#}$	4.37 (0.07)					0.48 (0.13)		
Theory (α_c=0)	5.61 [4.3]*	4.59 [5.0]	4.48	1.91	1.75	1.63	0.369 [23.1]	0.354	0.367
Theory (α_c=1)	6.59 [22.5]	4.90 [12.1]	4.66	2.20	1.89	1.67	0.382 [20.4]	0.353	0.375

[ ]*=relative error; ( )$^{\#}$=standard deviation of the experiment

fabrics were made using D_y =177.8(Tex) (1 Tex=1 gram of the yarn in a length of 1000m) glass fiber yarns (fiber density ρ_f=2.54 g/cm3) on a flat bed weft knitting machine. The knitting parameters used were W=2(loops/cm) and C=2.5(loops/cm). Glass fiber yarn in the knitted fabric composite had a packing fraction K=0.45 /4/. The composite contained a fiber volume fraction of 0.095 /4/. On the other hand, based on Leaf and Glaskin's geometrical description of the plain weft knitted fabric, the fiber volume fraction of the composite is estimated as /5/

$$V_f = \frac{D_y L_s C W}{\rho_f A t} \times 10^{-5} \tag{1}$$

where t is the thickness of the composite measured in centimeters, A is the planar area of the composite over which W and C are measured, and L_s is the length of yarn in one loop of the unit cell which can be represented approximately by /5/

$$L_s \approx 4(ad)\varphi \tag{2}$$

where d is the yarn diameter, a and φ are calculated from Eqs. (2.1) and (2.3) of Ref. /1/. As both W and C are specified in a unit length of 1 cm, A=1 cm^2. Corresponding to t=0.06cm, the estimated fiber volume fraction using Eq. (1) is V_f=0.0933, being close to the measured one. Hence equation (1) will be used in the following calculations, which is particularly useful in parametric studies for predicting elastic properties of plain knitted fabric composites.

The elastic moduli predicted using equation (75) of Ref. /2/ are summarized in Table 1. The results indicate that for the glass fiber fabric reinforced epoxy matrix composite, the iso-stress approach to the mechanical properties is more accurate than the iso-strain approach. In the present case, the stiffness ratio between the two constituent materials is: E^m/E^f=0.049≈5%. Hence, a conclusion might be that when the smaller modulus ratio (i.e., the smaller value between E^m/E^f and E^f/E^m) is larger than 1%, the iso-stress approach should be applied to estimate the mechanical properties of a composite with knitted fabric reinforcement. When this ratio is even smaller (as in the case shown in the next section), a combined approach may be suitable.

Let us now consider the influence of the fabric geometry on the elastic property of the composite. One significant advantage of an analytical model for the description of the fabric geometry is that it makes such an investigation possible. It is well known that increasing the fiber volume fraction can enhance the elastic properties of knitted fabric composites. Equation (1) suggests that V_f can be increased in two different ways: 1) by increasing the linear density of the yarn, D_y, and 2) by increasing stitch density of knitted fabric, N=W×C. The elastic constants versus various these parameters are thus calculated and are graphically represented in Figures 1 through 4. The results in these

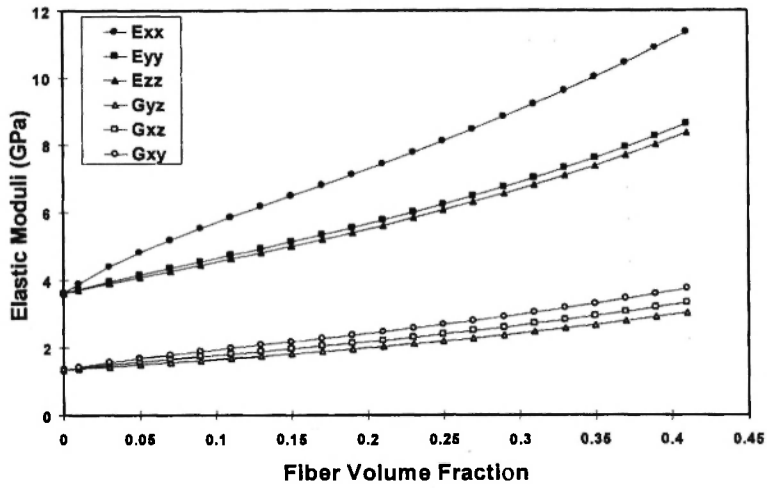

Fig. 1: Elastic moduli of plain knitted fabric composite versus fiber volume fraction. The parameters used are: E^f=74GPa, E^m=3.6GPa, ν^f=0.23, ν^m=0.35, D_y=177.8, C=2.5 loop/cm, W=2 loop/cm, and t=0.06cm.

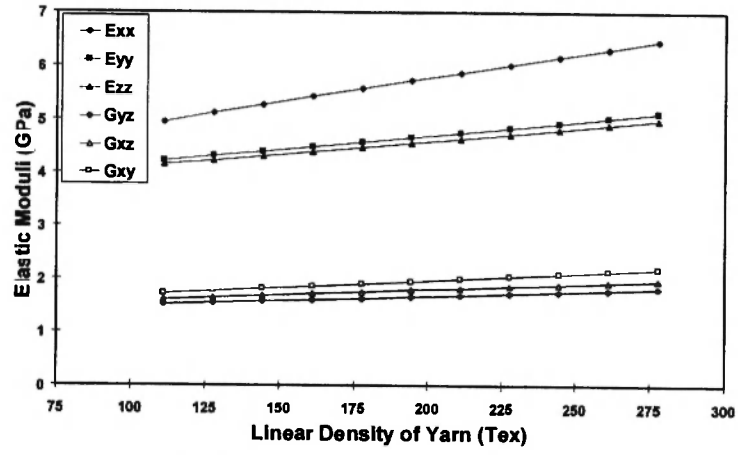

Fig. 2: Elastic moduli of plain knitted fabric composite versus the linear density of yarn (tex). The parameters used are: E^f=74.0GPa, E^m=3.6GPa, ν^f=0.23, ν^m= 0.35, C=2.5 loop/cm, W=2 loop/cm, and t=0.06cm.

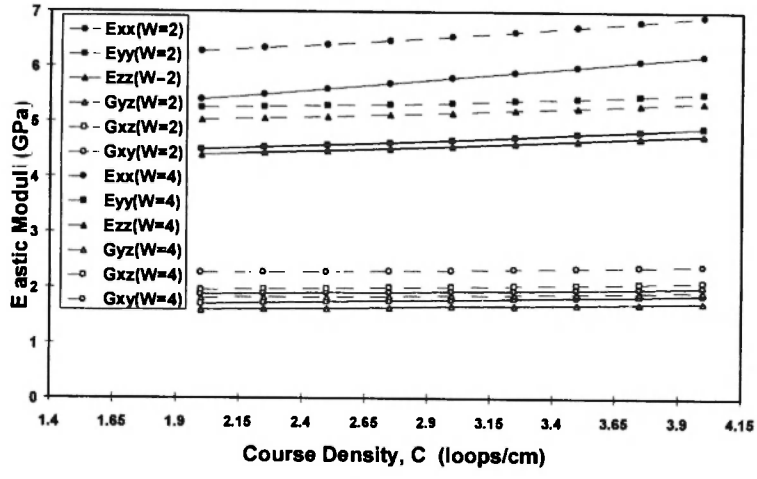

Fig. 3: Elastic moduli of plain knitted fabric composite versus course density of fabric. The parameters used are: E^f=74 GPa, E^m=3.6 GPa, ν^f=0.23, ν^m=0.35, D_y=177.8, and t=0.06cm.

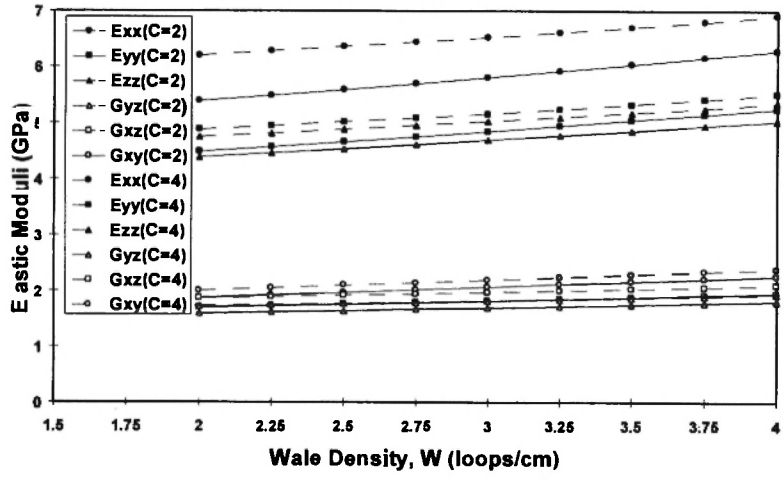

Fig. 4: Elastic moduli of plain knitted fabric composite versus wale density of fabric. The parameters used are: E^f–74GPa, E^m=3.6GPa,ν^f=0.23, ν^m=0.35, D_y=177.8, and t=0.06 cm.

figures are all computed on the iso-stress approach (α_c=0). Only the Young's moduli and the shear moduli are reported since the Poisson's ratios have shown little dependency on the fiber volume fraction V_f or other related parameters as long as V_f is not large.

The computed results indicate that the elastic moduli vary almost linearly with either of the parameters, yarn linear density (Tex), wale density (W), or course density (C), but vary slightly non-linearly with the fiber volume fraction of the composite.

2.1.2 Strength Simulation

Experimentally measured tensile strengths /4/ of the plain knitted fabric composite are listed in Table 2. No ultimate parameters of the glass fiber and the epoxy matrix were reported /4/. However, a UD composite lamina made from the same constituent materials has been tested /4/ and .the measured strengths in longitudinal and transverse directions are summarized in Table 3. From these data, the ultimate strengths of the fiber and the matrix can be back calculated, using equations (40.1)-(40.6) and (41.1)-(41.6) given in Ref. /2/. The recovering procedure is begun by assuming that the glass fiber is linearly elastic until rupture. As the stiffness of the fiber is much higher than that of the epoxy matrix (Table 1), we can imagine that the transverse tensile strength of the composite is governed by the strength of the matrix. Therefore, the equation (41.1) of Ref. /2/ gives

$$\sigma_{22}^{u}=\frac{\sigma_{Y}^{m}}{\alpha_{e2}^{m}}+\frac{\sigma_{u}^{m}-\sigma_{Y}^{m}}{\alpha_{p2}^{m}}=Y\approx\frac{\sigma_{u}^{m}}{\alpha_{e2}^{m}}, \tag{3}$$

since $\alpha_{p2}^{m}\sim\alpha_{e2}^{m}$. From Eq. (3), the matrix strength is determined to be 30.86MPa. Next, let us use the Eq. (40.1) of Ref. /2/ to recover the fiber strength. It is required that

$$\sigma_{11}^{u}=\min\left\{\frac{\sigma_{u}^{f}-(\alpha_{e1}^{f}-\alpha_{p1}^{f})\sigma_{11}^{0}}{\alpha_{p1}^{f}},\frac{\sigma_{u}^{m}-(\alpha_{e1}^{m}-\alpha_{p1}^{m})\sigma_{11}^{0}}{\alpha_{p1}^{m}}\right\}$$

$=X$

Table 2

Tensile Strength of Plain Knitted Fiber Fabric Composites. The used parameters are: E^f=74GPa, E^m=3.6GPa, ν^f=0.23, ν^m=0.35, E_T^m = 480MPa, σ_Y^m =20MPa, σ_u^f =1933MPa, σ_u^m =31.5MPa, d=0.0445cm, D_y=177.8Tex, K=0.45, ρ_f=2.54g/cm3, C=2.5loop/cm, W=2loop/cm, and t=0.06cm.

Load Direction	Strength of Composite (MPa)		Maximum Normal Stress (MPa)		Failure	
	Measured	Predicted*	Fiber	Matrix	Fiber	Matrix
Wale	62.83	65.40	408.53	31.51	No	Yes
Course	35.5	37.56	55.36	31.53	No	Yes

*predicted with $d\sigma$=0.06MPa.

Table 3

Tensile Strengths of Unidirectional Glass Fiber Epoxy Matrix Lamina (E^f=74Gpa, E^m=3.6GPa, ν^f=0.23, ν^m=0.35, E_T^m =480MPa, σ_Y^m =20MPa, σ_u^f =1933MPa, σ_u^m =31.5MPa, V_f=0.45)

Longitudinal Strength, X(MPa)		Transverse Strength, Y(MPa)	
Measured	Predicted*	Measured	Predicted*
885	887.18	45	44.8

*predicted with $d\sigma$=0.148Mpa

At this stage, we cannot assume that $\alpha_{p1}^{m}\sim\alpha_{e1}^{m}$. However, the longitudinal strength of the UD composite is most probably governed by the strength of the fiber. Thus, we can consider $X=\sigma_{11}^{u}\sim\frac{\sigma_{u}^{f}}{\alpha_{e1}^{f}}$, due to $\alpha_{p1}^{f}\sim\alpha_{e1}^{f}$, providing that we can choose the other two parameters of the matrix, E_T^m and σ_Y^m, such that

$$\left(\frac{\sigma_{Y}^{m}}{\alpha_{e1}^{m}}+\frac{\sigma_{u}^{m}-\sigma_{Y}^{m}}{\alpha_{p1}^{m}}\right)_{\sigma_u^m=30.86MPa}>X \tag{4}$$

It is obvious that many different combinations of E_T^m

and σ_Y^m, which satisfy inequality (4), exist. Hence, the recovered fiber strength is σ_u^f =1856.3MPa. Since $\left(\frac{\sigma_u^m}{\alpha_{\varepsilon 1}^n}\right)_{\sigma_u^m=30.86MPa} < X$, the epoxy used cannot be considered as linearly elastic until rupture. On the other hand, any combination of E_T^m and σ_Y^m, which satisfy (4), is possible as a result of no other information. However, use of different plastic parameters only results in slight differences of the retrieved strengths/ 6,8/. This may be attributed to the fact that the ultimate strength of the composite is mainly dependent on the ultimate stresses, but less on the yield stress or hardening modulus, of the constituent materials, although the ultimate strain and the entire stress-strain curve of the composite do depend on them. For this reason, we chose E_T^m =480MPa and σ_Y^m =20MPa in the remaining calculations. It is noted that slight amendments should be made for the ultimate strengths of the glass fiber and epoxy matrix when taking the matrix plasticity into account (the above estimations, σ_u^m =30.86MPa and σ_u^f =1856.3MPa, were based on no matrix plasticity). The recovered ultimate strengths of the constituents are given in Table 3. It is also noted that as in a laminate analysis the stresses shared by a lamina involved depend on the lamina strains (deformations), the exact matrix behavior should be employed.

Equations (76) and (77) of Ref. /2/ with α_c=0 have been applied to evaluate the stresses in the glass fiber and the epoxy matrix. No thermal or other kind of residual stress was assumed. The maximum normal stress criterion was then applied to check the failure status of the constituents at each updated load level. The predicted tensile strengths in the wale and in the course directions are given in Table 2. From these results, it is seen that the predictions are rather satisfactory.

Corresponding to the tensile strengths, the maximum normal stresses in the fiber and in the matrix are recorded and are also given in Table 2. These stresses clearly indicate that the failures of the composite, both in the wale and in the course directions, resulted from the failure of the epoxy matrix. This failure mode is consistent with the experimental observation /4/.

The influences of various parameters on the tensile strength of the plain weft knitted fiber fabric reinforced epoxy matrix composites are investigated and are graphed in Fig. 5 through Fig. 9.

Figs. 5(a) and 5(b) show the effect of increased yarn linear density on the composite strength and the maximum normal stresses in the constituent materials for the wale and course directions, respectively. From the figures, we can see that the strength of the composite in the course direction increases more than that in the wale direction, with the increase of the yarn linear density. Meanwhile, the maximum normal stress in the fiber decreases when loaded in the wale direction whereas it increases when loaded in the course direction. This is interesting but reasonable. According to equation (1), the fiber volume fraction, V_f, increases with the increase of the yarn linear density, D_y. However, this increased fiber volume fraction did not result in the significant increase of the composite strength in the wale direction. The reason is that the maximum normal stress in the fiber reduced significantly, see Fig. 5(a). It should be noted that the maximum normal stress in the matrix remained unchanged in all the cases. A similar phenomenon also appeared in Figs. 6(a) and 7(a). In all these cases, Figs. 5(a), 6(a), and 7(a), the applied load is in the wale direction. Fig. 6(a) shows a more interesting feature. With increasing course density, C, initially up to a threshold, 1.9, the maximum normal stress in the fiber increased, but above this threshold value it decreased. On the other hand, Figs. 6(b) and 7(b) indicate that the maximum normal stress in the fiber increases with the increase of the stitch density, $N=C\times W$, due to loads in the course direction, resulting in the increase of the overall strength of the composite in the same direction. It can be concluded from Figs. 5-7 that when the fiber volume fraction is increased through increasing the fabric stitch density, the overall strength of the composite as well as the maximum normal stresses in the constituent materials varies differently. The composite strength in the wale direction only varies slightly whereas the increase of the composite strength in the course direction is noticeable. In general, the maximum normal stress in the fiber reduces significantly under a wale load condition, whereas this stress enlarges only slightly if the load is applied along the course direction. As the matrix strength is too small and every such composite failure is always initiated by

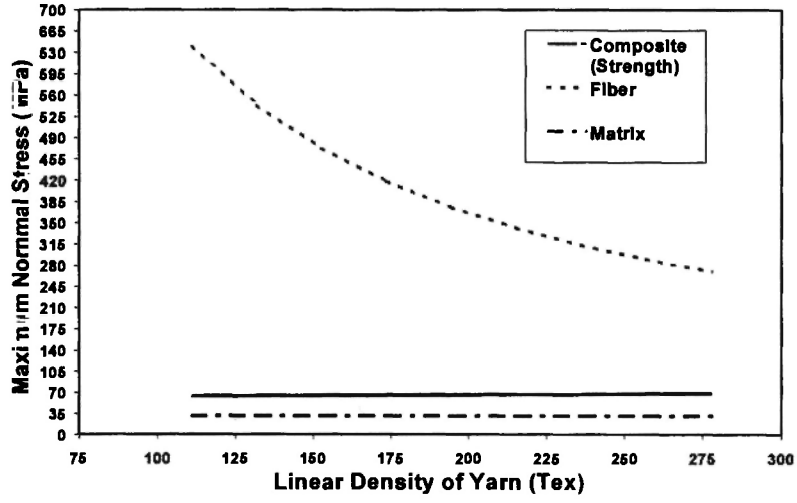

Fig. 5(a): Maximum normal stress in different phases versus the linear density of yarn under tensile load in wale direction. The geometric parameters used are: d= 0.0445cm, K=0.45, ρ_f =2.5g/cm^3, C=2.5 loop/cm, W=2 loop/cm and t=0.06cm.

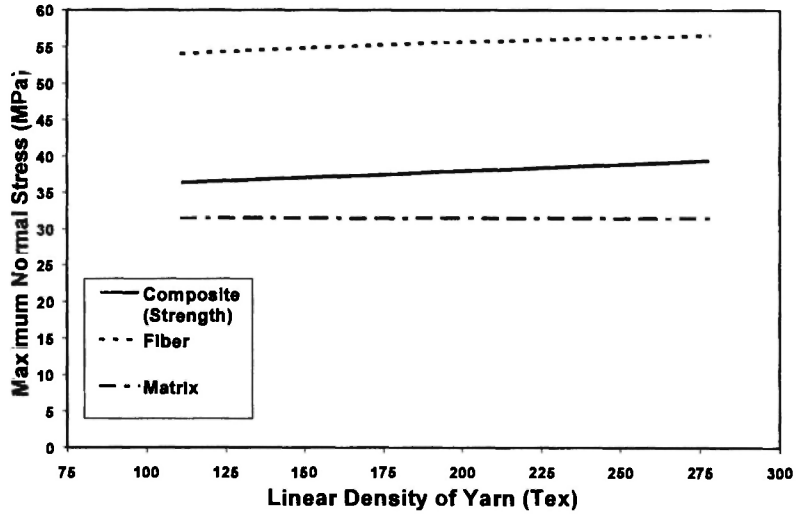

Fig. 5(b): Maximum normal stress in different phases versus the linear density of yarn under tensile load in course direction.

the matrix failure, the influence of the increased fiber volume fraction on the maximum normal stress in the matrix cannot be seen.

On the other hand, the fiber volume fraction can also be changed by varying the amount of matrix in the composite, for example, by changing the thickness of the composite. Figs. 8(a) and 8(b) indicate the influence of such change on the overall strengths of the composite in the wale and course directions, respectively. The qualitative conclusion drawn above also applies in these cases. Namely, with the increase of the fiber volume fraction, which corresponds to the decrease in the composite thickness, the maximum normal stress in the fiber reduces when loaded in the wale direction but enlarges if the load is applied in the course direction. However, the quantitative difference between the two cases, i.e., the increase of the fiber volume fraction by changing fabric stitch density and by varying the matrix

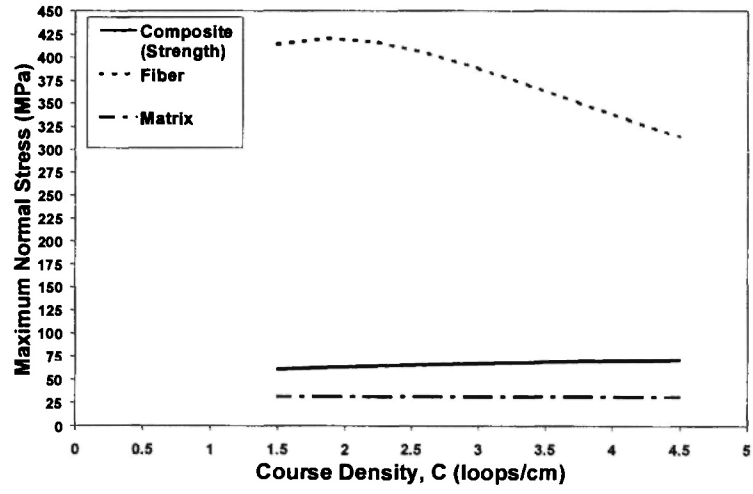

Fig. 6(a): Maximum normal stress in composite, fiber, and matrix *vs* the coursed density. The composite is loaded in wale direction. The geometric parameters used are: ρ_f = 2.54g/cm^3, d=0.0445cm, D_y=177.8(Tex), K=0.45, W=2loop/cm and t=0.06cm.

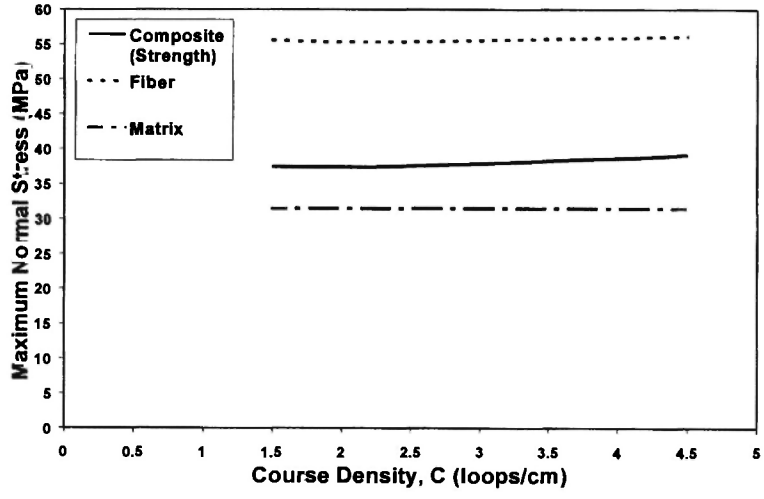

Fig. 6(b): Maximum normal stress in composite, fiber, and matrix *vs* the course density. The composite is loaded in course direction.

content, is noticeable. In the former case, the resulting increase in the composite strength is almost linear, whereas in the latter case, the influence of the matrix content on the composite strength appears to be nonlinear.

Finally, the influence of matrix strength on the overall composite strengths in the wale and course directions is shown in Figs. 9(a) and 9(b), respectively. The composite strengths in both the wale and course directions increased linearly with the increase of the matrix strength and at the same time the maximum normal stress in the fiber also increased linearly.

As a whole, the calculated results indicate that the tensile strengths of the composites are increased almost linearly with the increase of the linear density of the fiber yarn (D_y), the fiber volume fraction, which is inversely proportional to the composite thickness, and the stitch density (N=C×W). These phenomena are

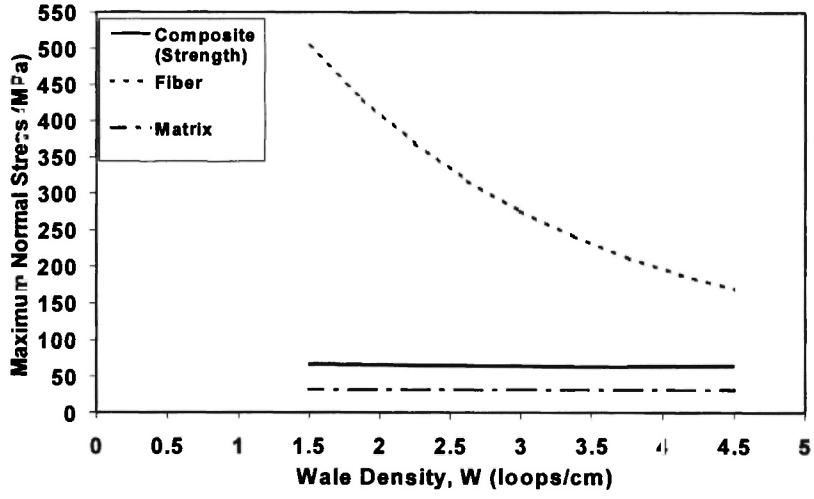

Fig. 7(a): Maximum normal stress in composite, fiber, and matrix *vs* the wale density. The composite is loaded in wale direction.The geometric parameters used are: ρ_f =2.54g/cm^3, d=0.0445cm, K=0.45, D_y=177.8(Tex), C=2.5loop/cm and t=0.06cm.

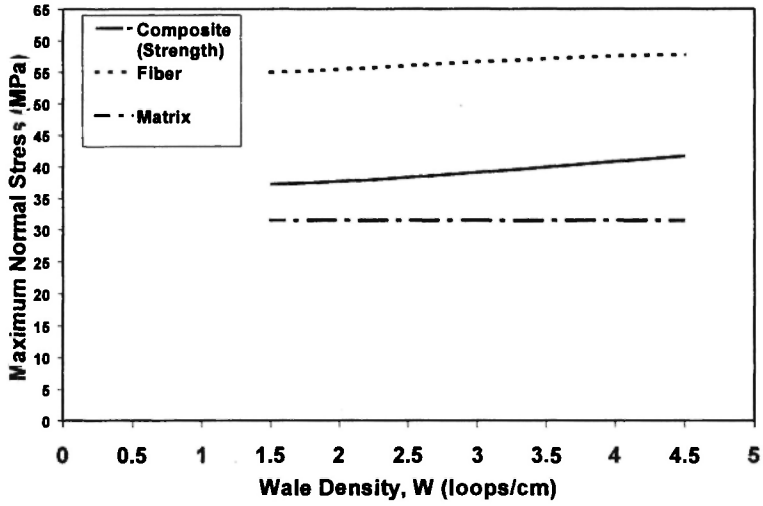

Fig. 7(b): Maximum normal stress in composite, fiber, and matrix *vs* the wale density. The composite is loaded in course direction

similar to those described for the elastic moduli of the composite, see Figures 1-4. Every parameter that affects the elastic modulus of the composite will also affect its tensile strength. It is to be noted that the ultimate strength of the epoxy matrix also plays a significant role in determining the strength of the composite. On the other hand, the elastic moduli (stiffnesses/compliances) of the composite do not depend on the ultimate strengths of the constituent materials.

For all the cases investigated, the composites failed due to the failure of the matrix, i.e., the maximum normal stress in the matrix always attained its ultimate value. On the other hand, the maximum normal stress in the fiber yarn varied dramatically with the parameters studied. To make full use of every constituent material in the knitted fabric composites, we may consider enlarging the maximum normal stress in the fiber. This can be achieved through several different ways. The

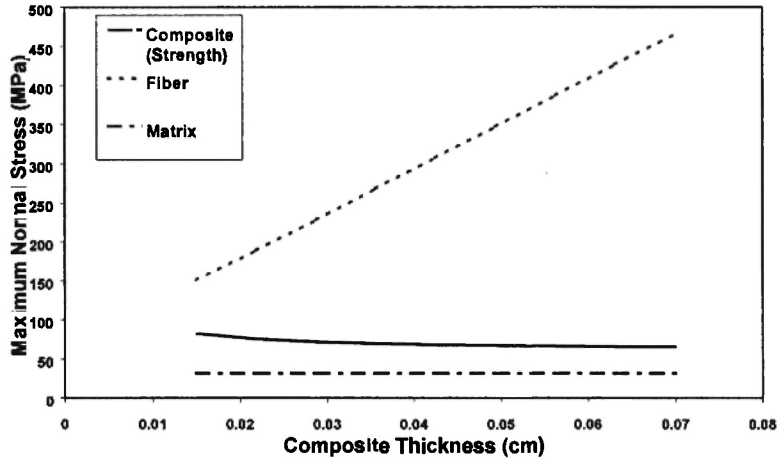

Fig. 8(a): Maximum normal stress in composite, fiber, and matrix *vs* the thickness of the composite,which is loaded in wale direction.The geometric parameters used are: d=0.0445cm, D_y=177.8(Tex), K=0.45, ρ_f=2.54g/cm^3, C=2.5loop/cm, and W=2 loop/cm.

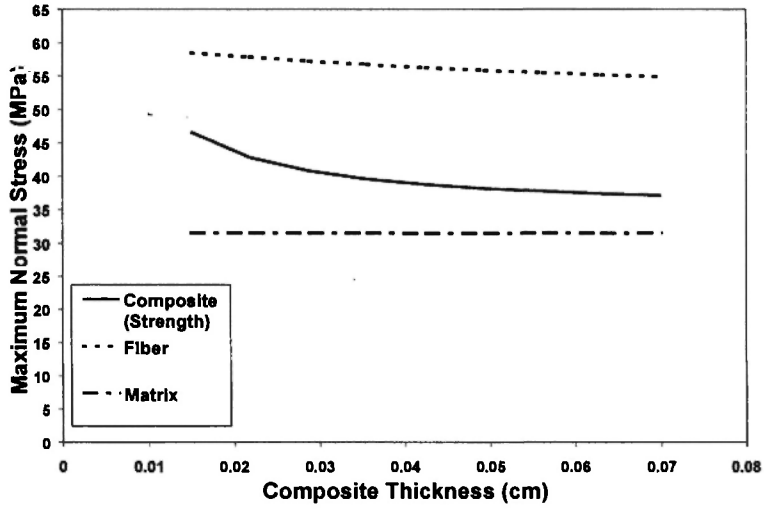

Fig. 8(b): Maximum normal stress in composite, fiber, and matrix vs the thickness of the composite, which is loaded in course direction

most efficient ways include: a) reducing the linear density of the yarn, b) decreasing the wale density of the fabric, c) increasing the thickness of the composite, and d) increasing the strength of the used matrix, as indicated in Figs. 5(a), 7(a), 8(a), 9(a), and 9(b). However, the increase of the fiber maximum normal stress should not sacrifice the overall strength of the composite to a significantly lower level. In regard to this, the increase of the composite thickness (without changing any fabric parameters) is not a good way.

2.2 Milano Rib Knitted Fabric Composites

Experimentally measured tensile properties of this type of fabric composites with different stitch structures shown in Table 2 of Ref. /1/ were reported in Ref. /9/. They are summarized in Table 4.

The fiber used was E-glass. Its properties are summarized in Table 5. The properties of the epoxy matrix used, however, were obtained through experiment. It is known that properties of polymer

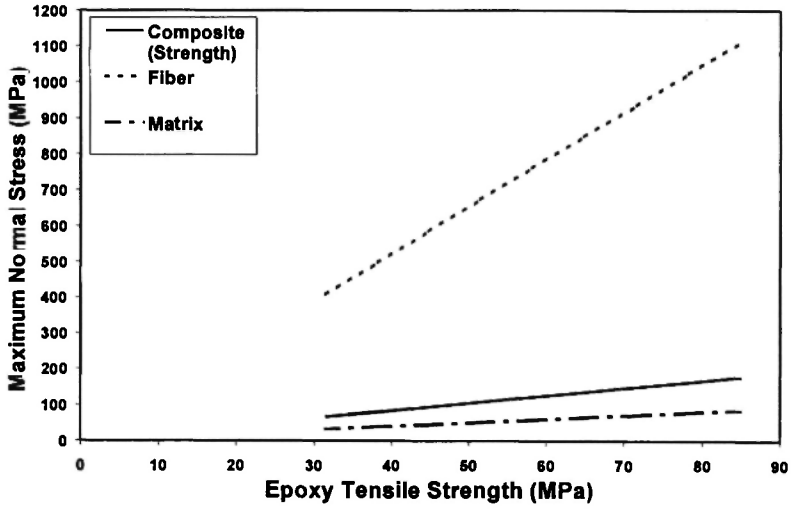

Fig. 9(a): Maximum normal stress in composite, fiber, and matrix *vs* the tensile strength of the matrix.The composite is loaded in wale direction.The geometric parameters used are: d=0.0445cm, D_y=177.8(Tex),K=0.45, ρ_f =2.54g/cm^3, C=2.5loop/cm, W=2.5loop/cm, t=0.06cm.

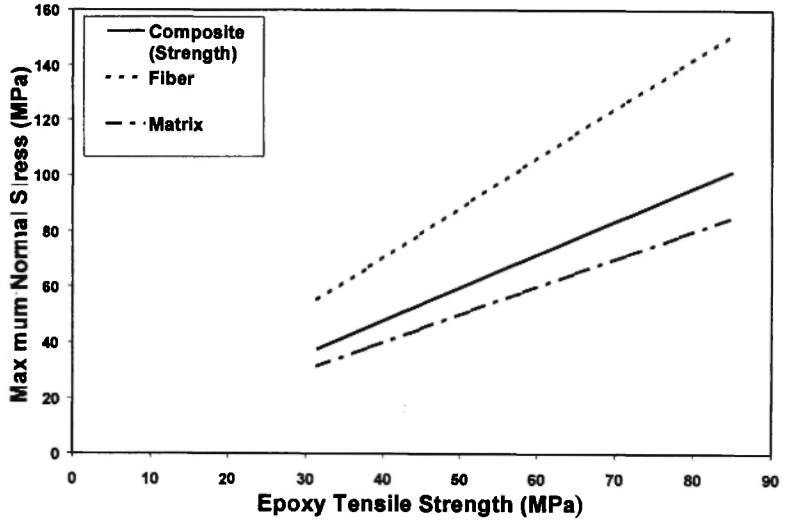

Fig. 9(b): Maximum normal stress in composite, fiber, and matrix *vs* the tensile strength of the matrix. The composite is loaded in course direction.

Table 4

Measured tensile properties of the fabric composites

Fabric type	Tensile modulus (GPa)		Poisson's ratio (ν_{xy})	Tensile strength (MPa)	
	Wale direction (E_{xx})	Course direction (E_{yy})		Wale direction ($\sigma^c_{u,xx}$)	Course direction ($\sigma^c_{u,yy}$)
M1	14.3	12.3	0.341	134.0	83.0
M3	14.9	13.2	0.342	122.0	82.8
R3	14.7	14.0	0.310	96.0	75.8

Table 5
Properties of the constituent materials

Materials	E (GPa)	ν	σ_Y (MPa)	E_T (GPa)	σ_u (MPa)
Glass fiber	74	0.23	1933	74	1933
Epoxy matrix	3.32	0.358	16.7	2.36	38.5

resins depend on hardeners used as well as on *in situ* processing conditions. Five tensile specimens of the monolithic matrix were prepared from a flat panel made using resin transfer molding method similarly as in fabricating the Milano rib knitted fabric composites. Two pieces of strain gauges were used to record longitudinal and transverse strains of each specimen, respectively. Typical stress-strain curves of the epoxy matrix in the longitudinal and transverse directions under uniaxial tension are shown in Fig. 10. Averaged test results from the five tensile specimens are listed in Table 5.

The geometrical description for the Milano rib knitted fabrics has been presented in Ref. /1/. A unit cell geometry for M3 fabric was shown in Fig. 34 of Ref. /1/. The unit cell geometries for the other type of Milano fabrics listed in Table 2 of Ref. /1/ can be determined similarly. After discretization of each unit cell (or, a RVE for the corresponding Milano fabric composite), the compliance and internal stress formulae similar to the equations (75)-(77) of Ref. /2/ can be obtained. Like the analysis of plain knitted fabric composites, the iso-stress approach (α_c=0) is employed. It may be noted that the compliance matrix and the stress formulae obtained are two-dimensional, as the Milano fabric geometry has already been approximated two-dimensionally. Thus, the in-plane response formulae as given in sub-section 3.5 of Ref. /2/ together with in-plane coordinate transformation matrices should be employed. A further remark is that each discretized sub-element of the RVE of a Milano rib knitted fabric composite contains more than two yarn segments, as can be seen from Fig. 34 of Ref. /1/. However, each yarn segment is still taken as a unidirectional composite, with a volume fraction equal to the overall fiber volume fraction of the Milano fabric composite. Therefore, with the same number of sub-elements, the RVE of a Milano rib knitted fabric composite has more sub-volumes than the RVE of a plain knitted fabric composite does.

Using the constituent parameters given in Table 5 and the fabric unit cell geometries, the predicted stiffness and tensile strengths of the two Milano and one rib knit fabric composites are given in Table 6. Comparing Table 6 with Table 4, we can see that the estimated stiffness and tensile strength of the three fabric composites are reasonably satisfactory. The slight discrepancy between the predicted and measured course direction stiffness and strength is attributed to the

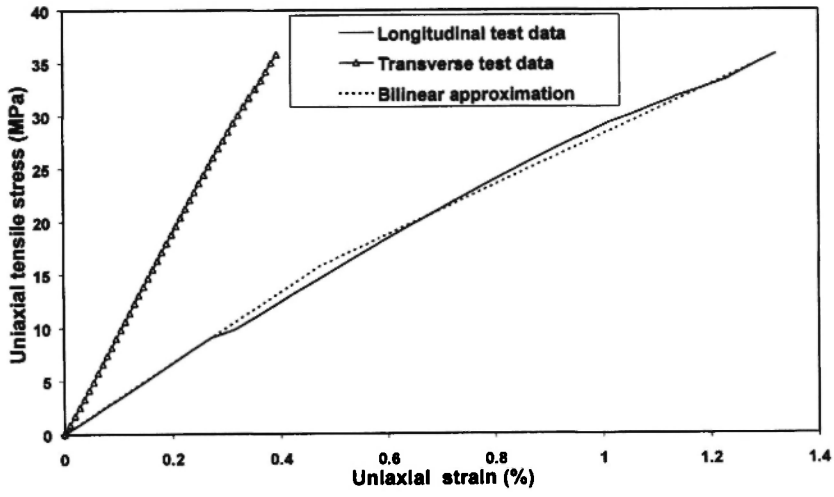

Fig. 10: Typical uniaxial tensile stress-strain curves of the neat epoxy matrix as used in Milano rib knitted fabric composites

Table 6
Predicted tensile properties of Milano rib knitted fabric composites

Fabric type	Stiffness calculation				Strength calculation (MPa)					
	E_{xx} (GPa)	E_{yy} (GPa)	G_{xy} (GPa)	ν_{xy}	Load in wale direction			Load in course direction		
					σ_f^1	σ_m^1	$\sigma_{u,xx}^c$	σ_f^1	σ_m^1	$\sigma_{u,yy}^c$
M1	17.4	10.9	5.43	0.407	153.4	38.5	120.8	83.0	38.5	64.7
M3	17.7	11.2	5.61	0.404	149.2	38.5	120.8	83.4	38.6	65.5
R3	15.3	10.9	5.07	0.404	154.8	38.6	103.0	87.9	38.6	65.2

inaccurate description for the fabric geometry. On the other hand, slightly better prediction can be achieved if we replace $|x_n - x_{n-1}|$ in Eqs. (69) and (73) of Ref. /2/ using $\sqrt{(x_n - x_{n-1})^2 + (y_n - y_{n-1})^2}$ where (x_{n-1}, y_{n-1}) and (x_n, y_n) are the planar coordinates of both the end points of the yarn segment under consideration. Namely, the assemblage along the fiber yarn direction could gain a better prediction in this case. It may be noted that the z coordinates of the end points would have been also included in the segment length calculation if we averaged along the yarn axial direction. However, due to the approximated geometric description for the knitted fabrics used in this study, the yarn orientation in the z direction has not been accurately identified and should not be incorporated.

Corresponding to the tensile strengths, the maximum normal stresses in the fiber and in the matrix are computed and are also given in Table 6. These stresses clearly show that the failure of the composite, either in the wale or in the course direction, resulted from the failure of the epoxy matrix. This failure mode has also been recognised during the experiments /10/. As the maximum normal stress in the fiber phase is much lower than the corresponding fiber ultimate tensile strength when the composite fails (see Table 6), the matrix strength plays a dominant role for the ultimate property of the knitted fabric reinforced composites. Any improvement in the matrix strength will increase directly the ultimate tensile strength of the resulting knitted fabric composite, whereas increasing the fiber strength will have no effect on the overall strength of the composite. On the other hand, the overall stiffness of the composite has a large dependency on the stiffness of the fiber material used. These observations are believed to be useful for the design of the knitted fabric reinforced composites.

A parametric study for the Milano rib knitted fabric reinforced composites could also have been performed. However, as the fabric geometries have been described using the Leaf and Glaskin model, the influence of the fabric geometric parameters on the stiffness and strength of the Milano rib knitted fabric composites would be very similar to that of the plain knitted fabric composites.

3. ELASTOMER MATRIX COMPOSITES

Composites made from various kinds of fibers and elastomer or rubber-like matrix materials have found a wide range of applications in engineering. The unique feature of the elastomer-based composites is that they can exhibit usable range of deformations much larger than those of the composites made using stiffer matrices, such as metals, ceramics, or rigid polymers. Composites made from knitted fabric and elastomer matrix can be good candidates in bio-engineering applications /11/. The real potential of the elastomer-based composites can be assessed only if their mechanical properties have been fully understood.

In order to analyze the nonlinear response characteristics of elastomer-based composites, previous researchers have mainly treated them as grossly anisotropic bodies /12-21/ capable of finite-elastic deformation. Various strain energy functions were used to correlate the stresses and strains generated in the composites. The material parameters involved in these

functions have to be determined experimentally.

The earliest investigation on the large deformation of a fiber reinforced rubber material was carried out by Adkins and Rivlin /13/. They developed an "ideal fiber reinforced composite" model, which was based on the assumptions of volume incompressibility and fiber inextensibility. The strain energy was taken to be that of an isotropically elastic rather than a transversely isotropic material. The model could not predict the mechanical properties of the composites from the properties of their constituents. The same ideal was also applied by Pipkin and Rogers /14/ and by Spancer /15/.

Hahn /16/ and Hahn and Tsai /17/ employed a complementary energy function to derive the stress-strain relation of the composites in finite deformation. In their equations, only the relationship between shear stress and shear strain is nonlinear whereas the tensile properties are linear. Jones and Morgan /18/ proposed an elastic energy function to describe the nonlinear response characteristics of an orthotropic material. These models do not lay emphasis on the particular fiber geometry.

Recently, Chou and his co-workers developed a nonlinear and finite deformation constitutive model for the wavy fiber reinforced elastomeric composites /19-21/. A complementary energy function was used and the overall strains (either in Eulerian or in Lagrangian system) generated in the composites were connected with the overall stresses in a set of nonlinear equations similar to those used by Hahn and Tsai /17/. The fiber finite deformations were obtained through geometrical analysis. The material parameters involved in the energy function had to be determined through experiments on a unidirectional composite.

It is clear that all the above-mentioned models treated rubber-based composites as a whole, whereas the material constants in the models have to be determined through experiments on the composites rather than on the constituent materials. In this work, the bridging model combined with the incremental rubber elasticity theory summarized in Ref. /2/ has been applied to estimate the entire stress-strain relationship of an elastomeric composite. The analysis is micromechnical, i.e. only constituent properties have been used as input parameters.

3.1 Constituent Properties

The composite under study was fabricated using an interlock polyester fiber fabric and a polyurethane elastomer matrix. The geometry of a representative volume element (RVE) for this composite has already been identified in Section 3.2 of Ref. /1/. Its constituent properties, obtained experimentally using monolithic material specimens, are summarized below.

The polyester fiber used can be considered as isotropic and bilinearly elastic-plastic, having the following uniaxial tensile stress-strain relationship /22/

$$\sigma = \begin{cases} E^f \varepsilon, & when \quad 0 \le \varepsilon \le \varepsilon_Y^f \\ \sigma_Y^f + E_T^f \left(\varepsilon - \varepsilon_Y^f\right), & when \quad \varepsilon_Y^f \le \varepsilon \le \varepsilon_u^f \end{cases} \tag{5}$$

The other material parameters including Poisson's ratio are listed in Table 7. Thus, the instantaneous compliance matrix of the polyester fiber material can be described using the Prandtl-Reuss theory.

On the other hand, the polyurethane matrix used is a rubber-like material, having a uniaxial tensile stress-strain curve shown in Fig. 11. Applying equations (47)-(49) of Ref. /2/, the load dependent Young's modulus of the polyurethane can be represented in terms of the effective strain as /23/

Table 7
Material Properties of Polyester Fiber Yarn /22/

E_L (GPa)	E_T (GPa)	σ_Y (MPa)	σ_u (MPa)	ε_Y (%)	ε_u (%)	ν
6.044	2.298	104.8	323.9	1.734	11.268	0.42

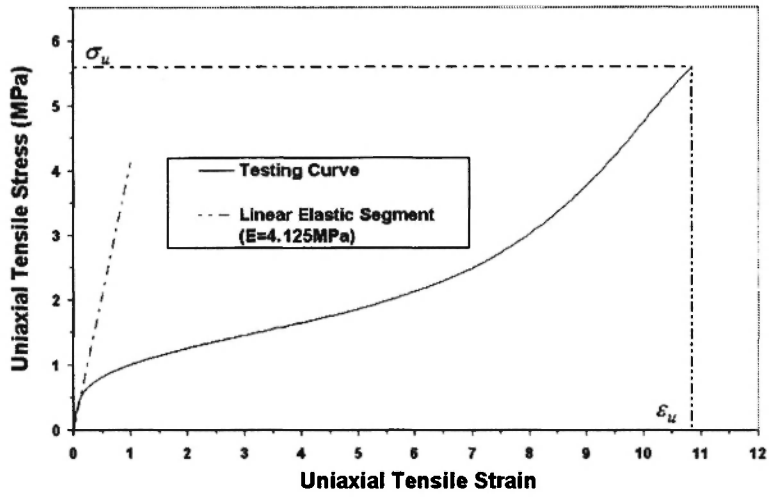

Fig. 11: Typical tensile stress-strain curve of a polyurethane elastomer

$$E_m(\varepsilon_e)=A_1+A_2(\varepsilon_e-\varepsilon_o)+A_3(\varepsilon_e-\varepsilon_o)^2+ \cdots + A_{18}(\varepsilon_e-\varepsilon_o)^{17}, \quad \varepsilon_e \le \varepsilon_{eu} \tag{6}$$

where A_1=+0.265953E+00,
A_2=+0.664798E-01,
A_3=-0.379756E-01,
A_4=+0.466002E-01,
A_5=+0.948304E-01,
A_6=-0.312507E-01,
A_7=-0.463988E-01,
A_8=+0.113865E-01,
A_9=+0.110157E-01,
A_{10}=-0.231237E-02,
A_{11}= -0.140701E-02,
A_{12}=+0.270237E-03,
A_{13}=+0.987754E-04,
A_{14}= -0.180004E-04,
A_{15}=-0.358759E-05,
A_{16}=+0.632672E-06,
A_{17}=+0.526406E-07,
A_{18}= -0.909288E-08, and
ε_o= 4.4566 and ε_{eu}=8.84.

In the above, the unit for all the A_i's is MPa; ε_o is an averaged strain and ε_{eu} represents the ultimate effective strain of the polyurethane. Similarly, the Poisson's ratio is found to be /23/

$$\nu_m(\varepsilon_e)=B_1+B_2(\varepsilon_e-\varepsilon_o)+B_3(\varepsilon_e-\varepsilon_o)^2+ \cdots + B_{18}(\varepsilon_e-\varepsilon_o)^{17}, \quad \varepsilon_e < \varepsilon_{eu} \tag{7}$$

where B_1=+0.307893E-01,
B_2=-0.886663E-02,
B_3=+0.213949E-02,
B_4=-0.487063E-03,
B_5=+0.952827E-04,
B_6=-0.149274E-04,
B_7=+0.869008E-05,
B_8=-0.361783E-05,
B_9=-0.808093E-06,
B_{10}=+0.508998E-06,
B_{11}=+0.135182E-06,
B_{12}=-0.640060E-07,
B_{13}=-0.859589E-08,
B_{14}=+0.398899E-08,
B_{15}=+0.316317E-09,
B_{16}=-0.138212E-09,
B_{17}=-0.327201E-11,
B_{18}=+0.172326E-11.

Comparisons between the experimentally determined and the polynomial approximated Young's modulus and Poisson's ratio are shown in Figs. 12 and 13, respectively.

3.2 Linear Response

At every load level, the polyurethane matrix is always isotropic and elastic. Its compliance matrix is simply defined by Hooke's law, with Young's modulus

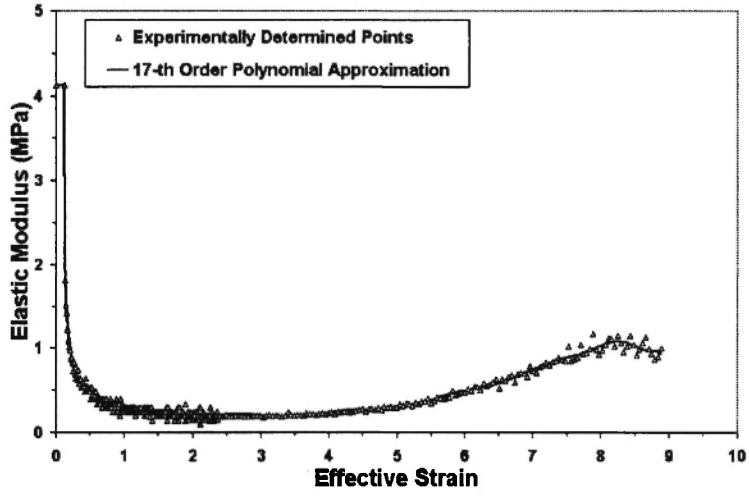

Fig. 12: Young's modulus of polyurethane versus effective strain

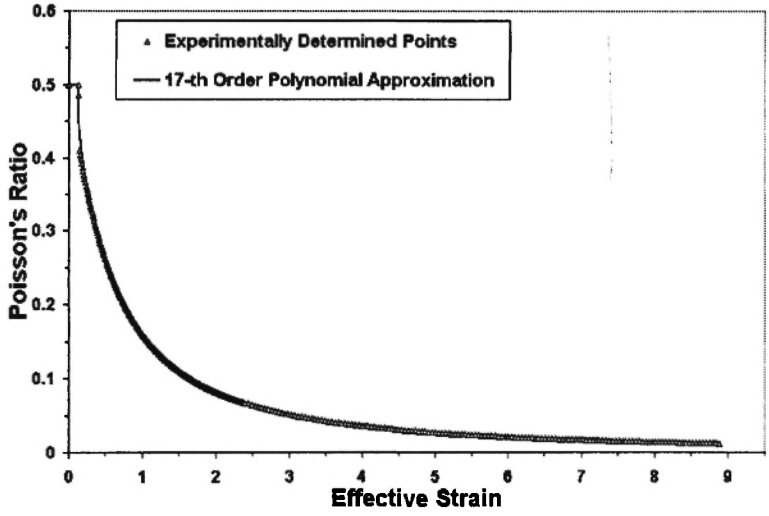

Fig. 13: Poisson's ratio of polyurethane versus effective strain

and Poisson's ratio given by equations (6) and (7). Its effective shear modulus is given by $G_m=E_m/(2(1+\nu_m))$. The instantaneous compliance matrix of the polyester fiber is also obtainable. Therefore, the bridging model, specifically equations (75)-(77) of Ref. /2/, can be applied.

First, the linear stress-strain response of the composite when loaded in either wale or course direction is calculated. An important step in the calculation is to choose the contribution ratio parameter of the iso-stress approach, α_s, used in equations (75)-(77) of Ref. /2/. The best way to do this is through experimental correlation. The measured stress-strain curve of the composite in a linear elastic range can be utilised for this purpose. Choosing different α_s, different composite moduli are calculated from equation (75) of Ref. /3/. Figs. 14 and 15 show some predicted linear stress-strain curves versus α_s (denoted by ALFs in the Figs.) for wale-direction and course-direction loaded composites, respectively. The experimentally measured curves are also plotted in the figures. From the figures, it can be seen that when $0.1\leq\alpha_s<0.15$, the predicted stress-strain curves, in both the wale and course directions, are in close neighbourhood of the

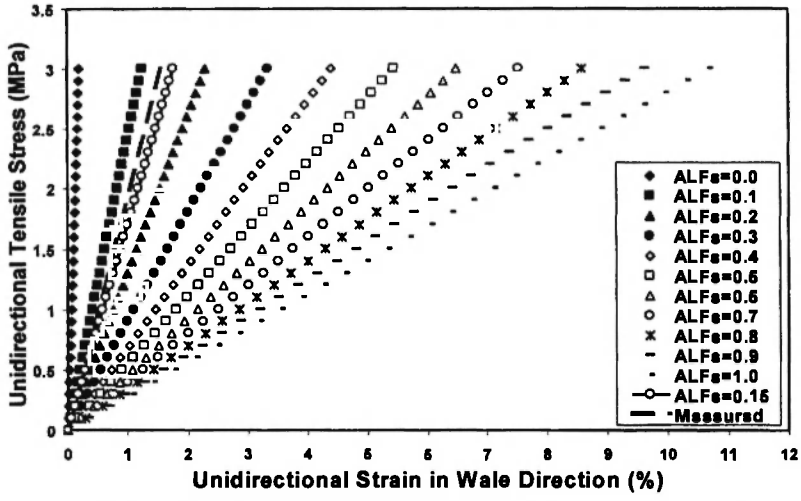

Fig. 14: Composite unidirectional σ_{xx}-ε_{xx} curves versus α_s (ALFs). The parameters used are: E^f=6.044GPa, E^m=4.125MPa, ν^f=0.42, ν^m=0.5, and V_f=0.362.

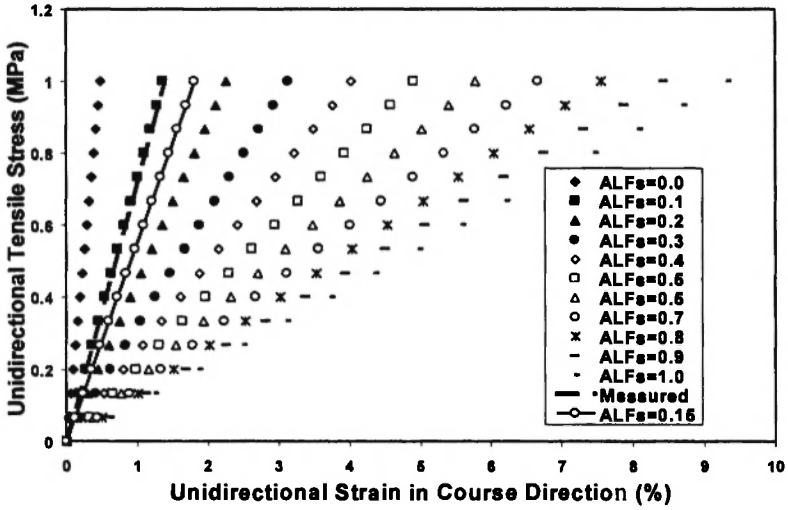

Fig. 15: Composite unidirectional σ_{yy}-ε_{yy} curves versus α_s (ALFs). The parameters used are: E^f=6.044GPa, E^m=4.125MPa, ν^f=0.42, ν^m=0.5, and V_f=0.354.

experimental data. Taking α_s=0.1 and 0.15, the calculated engineering moduli of the composite are listed in Table 8. The experimental data are also shown in the table. Comparison indicates that with α_s=0.1, the predicted elastic properties of the composite are in closest agreement with the experimental data both in wale and in course directions. This α_s will be used in the subsequent sections to estimate the nonlinear response of the composite.

3.3 Nonlinear Response

There are two important issues that need to be addressed in the nonlinear calculations. First, the Young's modulus and Poisson's ratio of the matrix are no longer constant, but are computed using equations (6) and (7). Second, the fiber yarn coordinates in the unit cell are not fixed, as a result of the significant geometrical changes in the knit loops during

Table 8

Predicted and measured engineering moduli of the knitted fabric reinforced elastomer composite. The parameters used are: E_f=6.044GPa, E_m=4.125MPa, ν_f=0.42, ν_m=0.5, and V_f=0.362.

Method	E_{xx} (MPa)	E_{yy} (MPa)	E_{zz} (MPa)	G_{xy} (MPa)	G_{xz} (MPa)	G_{yz} (MPa)	ν_{xy}	ν_{xz}	ν_{yz}
Predicted (α_s=0.1)	241.2	74.50	79.69	31.86	29.61	29.60	0.598	0.395	0.813
Predicted (α_s=0.15)	169.6	56.28	60.05	22.55	29.57	29.57	0.590	0.406	0.803
Measured	192.43	71.4	-	-	-	-	-	-	-

deformation of the composite. The deformed yarn coordinates are updated according to /23/

$$x_i^Y = x_i^Y + (x_i^Y - x_0)d\varepsilon_x, \quad (8.1)$$

$$y_i^Y = y_i^Y + (y_i^Y - y_0)d\varepsilon_y \quad (8.2)$$

where (x_o, y_o) is the centre point of the unit cell, i.e., x_0=0.3021mm and y_0=0.3259mm (see Fig. 29 in Ref. /1/), and $d\varepsilon_x$ and $d\varepsilon_y$ are the overall strain increments in the wale and course directions, respectively.

At each loading step, the calculated internal stresses in the polyester fiber and the polyurethane matrix are checked against their measured ultimate stresses, 323.9MPa and 5.59MPa /23/. All the predictions for different cases have indicated that the composites fail due to matrix failure, which agrees with the experimental evidences /23/.

The predicted stress-strain curves in the wale and course directions are plotted in Figs. 16 and 17, respectively. From these figures, the corresponding Young's moduli (E_L), knee stresses (σ_L), knee strains (ε_L), ultimate stresses (σ_u), and ultimate strains (ε_u) can be specified. They are listed in Table 9, in which the experimental data are also shown. It is seen that the predicted properties in wale direction are in good agreement with the experimental data. On the other hand, except for the Young's modulus, the other predicted properties in course direction are in less agreement with experimental results. However, Fig. 17 indicates that the predicted stress-strain curve in the course direction almost has a similar behavior to that of

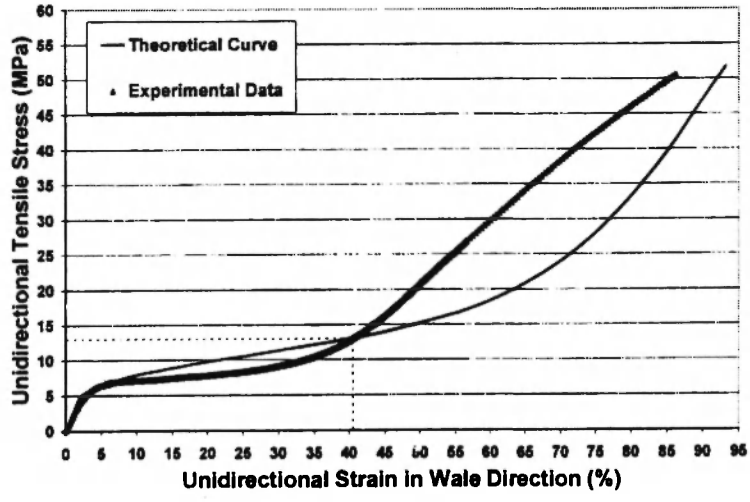

Fig. 16: Predicted and measured stress-strain curves of a knitted fabric reinforced elastomer composite in wale direction. The parameters used are: V_f=0.362, N=50, $d\sigma_x$=0.008MPa.

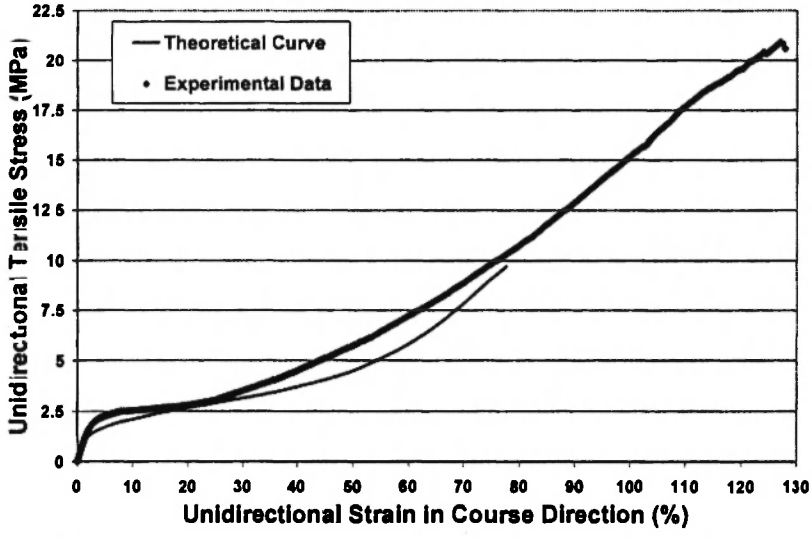

Fig. 17: Predicted and measured stress-strain curves of a knitted fabric reinforced elastomer composite in course direction with V_f=0.354, N=50, $d\sigma_y$=0.008MPa.

Table 9
Predicted and measured mechanical properties of the composite

Direction	Method	V_f	E_L (MPa)	σ_L (MPa)	σ_u (MPa)	ε_L (%)	ε_u (%)
Wale	Measured	0.362	192.43	4.05	50.52	2.10	86.23
	Predicted	0.362	241.2	4.65	51.67	1.93	93.19
Course	Measured	0.354	71.4	1.77	20.86	2.49	127.48
	Predicted	0.354	70.6	1.15	9.72	1.63	77.72

the experimentally determined curve within the estimated strain range. The predicted stress-strain curve in the wale direction, however, only agrees well with the experimental curve before a "threshold" strain, 40.53%, which is 47% of the actual ultimate strain. After this threshold value, the predicted results differ from measured data noticeably.

Comparing the predicted ultimate strain in the course direction, 77.72%, with experimentally measured ultimate strain, 127.48%, a conclusion may be drawn that the present micromechanical model is useful to estimate the stress-strain response characteristic of the knitted fabric reinforced elastomer composite in the strain range up to 50% of its ultimate strain. For the later part (another 50%) of the strain range, the present model gives inaccurate/incorrect results. This can be attributed to the intrinsic limitation of the mechanics of materials approach based on which the present model was developed. The equations (8) only determine the "averaged" co-ordinates of the displaced yarn loop, whereas the exact position of the yarn under an external load cannot be defined with the present model, because the composite "strain" has already been volume-averaged with respect to the RVE. It may be also noted that, due to the very large difference between the stiffnesses of the constituent materials, the overall mechanical properties of the composite are extremely sensitive to the fiber yarn orientation /21/. Hence, the inaccuracy in determining the displaced yarn coordinates under loading is a main source of error. However, it can be said that as long as the overall deformation of the composite is not very large (less than

Table 10
Predicted maximum normal stresses in constituent phases of the composite at failure

V_f	Uniaxial Load		Fiber		Matrix	
	σ_x (MPa) (Wale)	σ_y (MPa) (Course)	σ^f_{max} (MPa)	Failure	σ^m_{max} (MPa)	Failure
0.362	51.67	0	93.18	No	5.59	Yes
0.354	0	9.72	11.28	No	5.59	Yes

half of its deformation limit), the coordinate-updating formulae (8) are applicable and the predicted results are reasonably accurate.

Table 10 lists the stress levels in the two constituent materials when the composite failed due to uniaxial tensile loads in different directions. It can be seen that the maximum normal stress of the fiber is much lower than its ultimate stress, 323.9MPa. In other words, the fibers were not used to their full capacity. This information is useful for a composite designer to select alternative reinforcement fiber and matrix materials.

3.4 Parametric Study

Several parameters may influence the predictions of the composite, such as size of the applied load steps, $d\sigma_x$ and $d\sigma_y$, and the number of yarn segments in the unit cell (N-1). The effects of these parameters are summarised in Figs. 18 through 23. In general, as can be expected, the smaller the size of the load step, the more accurate are the predicted results. The estimated results in wale direction are more sensitive to the load increment than those in course direction. However, from Figs. 18 and 19 one can see that a further reduction in the stress step size beyond 0.008MPa yields little improvement in the accuracy of the predicted data. Therefore, all the other results reported were obtained based on a stress increment of 0.008MPa. Figs. 20 and 21 show the predicted data versus different number of discretized yarn segments. As a whole, the predictions do not depend significantly on the number of segments. It is seen that N=50, i.e., 49 discretized segments, already gave converged solutions both in wale and in course directions.

The final investigation is about the influence of the fiber volume fraction on the composite behaviors. For a given fabric geometry, the fabric stitch density and the yarn diameter were assumed to be unchanged. Hence,

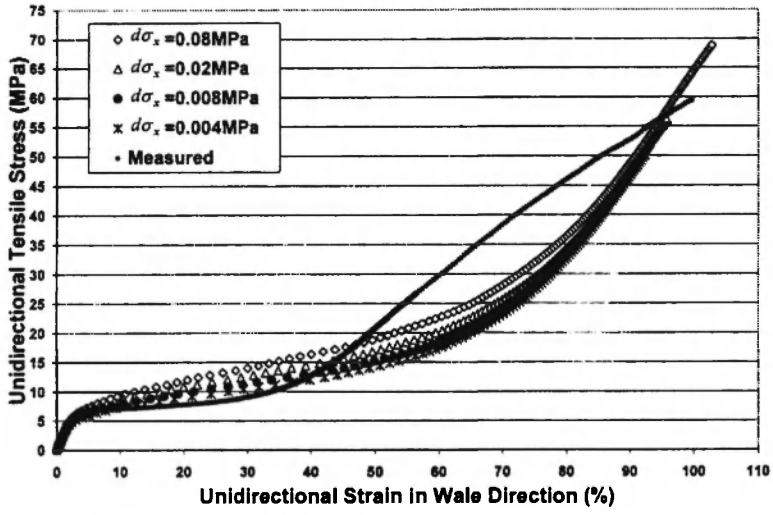

Fig. 18: Influence of size of stress step on predicted stress-strain curves in wale direction. The parameters used are: V_f=0.362 and N=50.

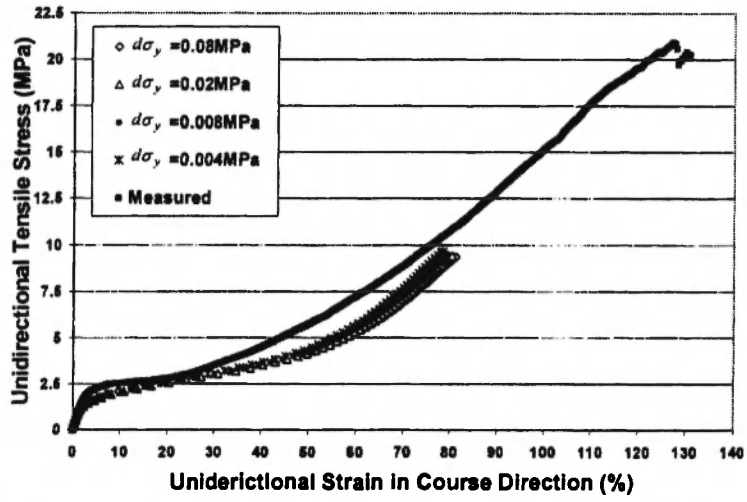

Fig. 19: Influence of size of stress step on predicted stress-strain curves in course direction. The parameters used are: V_f=0.354 and N=50.

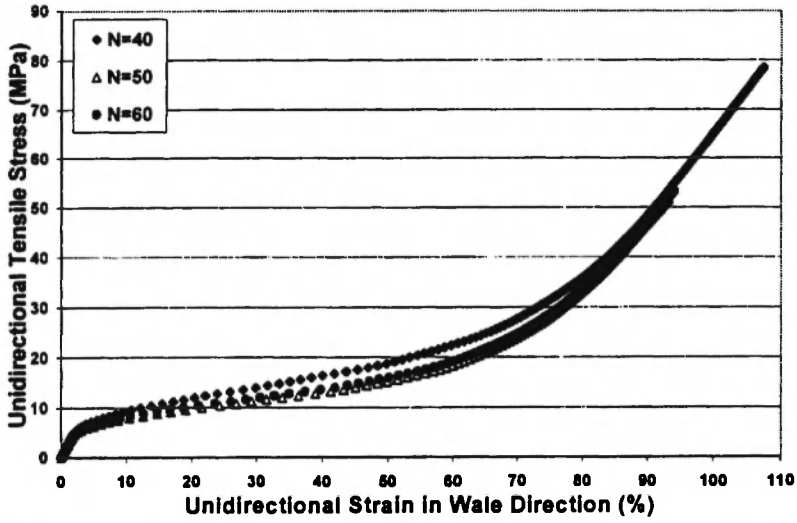

Fig. 20: Influence of discretized segments, (N-1), on predicted stress-strain curves in wale direction. The parameters used are: V_f=0.362 and $d\sigma_x$=0.008MPa.

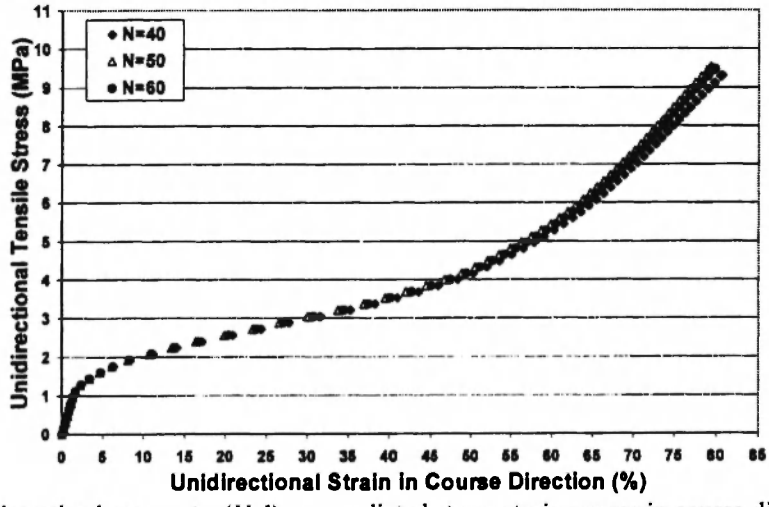

Fig. 21: Influence of discretized segments, (N-1), on predicted stress-strain curves in course direction. The parameters use are: V_f=0.354 and $d\sigma_y$=0.008MPa.

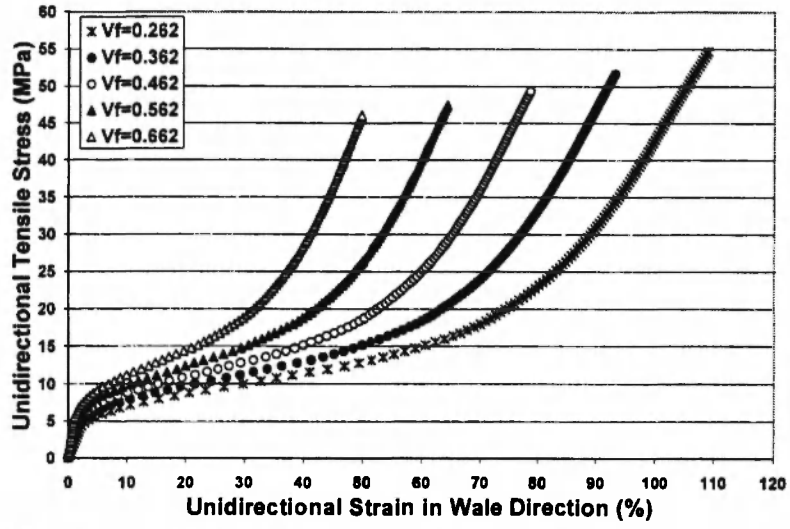

Fig. 22: Influence of fiber volume fraction, V_f, on predicted stress-strain curves in wale direction. The parameters used are: N=50 and $d\sigma_v$=0.008MPa.

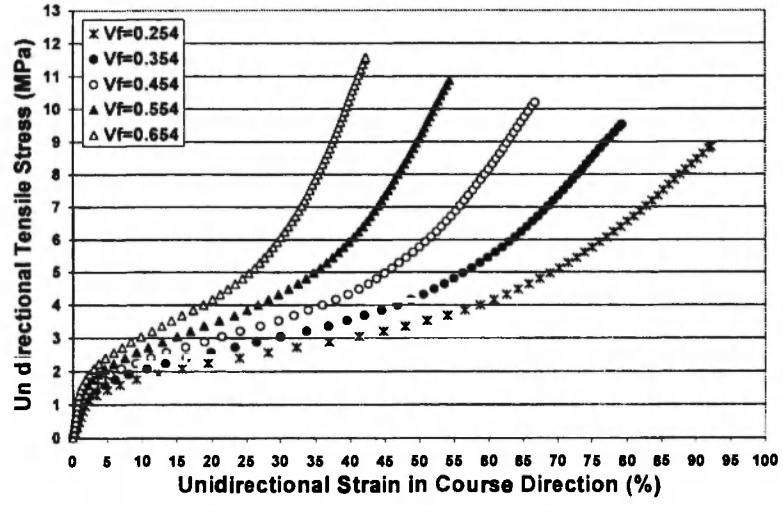

Fig. 23: Influence of fiber volume fraction, V_f, on predicted stress-strain curves in course direction. The parameters used are: N=50 and $d\sigma_v$=0.008MPa.

the variation of the fiber volume fraction could be introduced only by changing the thickness of the composite, i.e. by changing the volume of matrix. The response characteristics of the composite versus different fiber volume fractions are shown in Figs. 22 and 23 for wale and course directions, respectively. From both figures, one can clearly see that the overall response characteristics of the composite are sensitive to the fiber volume faction. The composite becomes more compliant and the overall ultimate strain of the composite becomes larger as the fiber volume fraction decreases. This is consistent with the experimental observations.

4. LAMINATED COMPOSITES

Most structural components of composite materials in engineering applications consist of multilayer composite laminates to meet specific structural requirements. This is also true for knitted fabric composites. In order to identify the structural safety,

knowledge of strength of the multilayer knitted fabric reinforced laminates is necessary. Prediction of this strength is thus of great importance in adequate design of the composite laminates and in development of material systems. It has been recognized that the failure analysis and ultimate strength prediction of composite laminates is difficult in nature and has not been well addressed in the literature /24/. A key problem involved is that the load share by each lamina ply in the laminate depends on the instantaneous stiffness matrix of the lamina, which is not a constant up to lamina failure in most cases /25/. Although a number of failure criteria have been established in the literature for UD laminae or for constituent fiber and matrix materials, none of them can result in an accurate prediction for the laminate strength if the load shared by the lamina in the laminate is inaccurately determined. It appears that, by using the Bridging Model, the lamina instantaneous compliance matrix can be easily defined. Combining this model with the classical lamination theory, the progressive failure process in the laminates can be identified and the laminate ultimate strength subjected to any arbitrary load condition can be determined /26/.

4.1 Experimental Evidence

E-glass fiber yarns of 600 Tex with a mass density of ρ=2.54g/cm3 were used to prepare plain weft knitted fabrics on a manual Flying Tiger knitting machine. Stitch densities of W=4.0loop/cm and C=3.2loop/cm were used in the fabric preparation. However, these parameters changed slightly after the composite fabrication. The stitch density that was indicated in Table 11 was an averaged measurement from the composite panels. The matrix used was a mixture of an epoxy resin R-50 and hardener H-64 (100 to 48 in ratio of weights) from Chemicrete Enterprises Pte. Ltd (Singapore). A hand lay-up method was employed to fabricate the composite laminates. Four fabric lay-ups were employed, i.e., [0/0/0/0/], [0/45/-45/0], [0/90/90/0], and [90/90/90/90], where 0-direction refers to the fabric wale direction (refer to Fig. 7 of Ref. /2/). The composite panels with no observable defects were used to prepare tensile specimens. A flat panel of monolithic matrix material was also made under the same condition as that used in making the composite materials. All the specimens had a width of 25mm and a gauge length of 150mm, with a thickness in between 4.07-4.55mm.

Five or four specimens were tensile tested for the composite of each fabric configuration, using an Instron testing machine (Type 8505), at a cross head speed of 1.5mm/min. Averaged stiffness and strength of each composite were obtained based on the machine records. Namely, the strains were calculated from the cross-head displacements divided by the original gauge length, although strain gauges were also used to measure Poisson's ratio of monolithic specimens. This is because the length of a strain gauge could only cover a limited number of knitted fabric loops, which might not be enough for an accurate measurement of the composite strains. The averaged test results are summarised in Table 11. In the table, the fiber volume fraction of each composite was obtained using a combustion method. Tensile tests were also performed for the monolithic matrix specimens. Averaged properties of the matrix

Table 11

Measured tensile properties of plain knitted E-glass fiber fabric reinforced epoxy laminates. The constituent parameters are: E^f=74 GPa, ν^f=0.23, E^m=2.32GPa, ν^m=0.42, E_T^m =527MPa, σ_Y^m =27MPa, σ_u^f =1933MPa, σ_u^m =39.2MPa, C=3.46cycles/cm, W=3.86cycles/cm and d=0.0586cm.

Laminate lay-up	V_f	Modulus in load direction (GPa)	Ultimate strength (MPa)	Load direction
[0/0/0/0]	0.226	6.64	100.4	Wale (0)
[90/90/90/90]	0.235	4.75	44.89	Course (90)
[0/90/90/0]	0.210	5.50	60.0	Wale (0)
[0/45/-45/0]	0.217	6.25	69.01	Wale (0)

materials are listed in Table 11, in which the Poisson's ratio was obtained from two strain gauge measurements. For the E-glass fibers used, their properties were taken from Ref. /6/, and are given in Table 11.

4.2 Simulation Results

The simulation procedure described above has been applied to estimate tensile properties of four plain weft knitted fabric reinforced laminates subjected to a uniaxial tension load. The fabrics are respectively placed in $[0]_4$, $[90]_4$, [0/90/90/0], and [0/45/-45/0] lay-up configurations. All the fabrics have the same stitch parameters, but the thicknesses of the composite panel made using different lay-up configurations are different, leading to different fiber volume fractions. Each lamina layer in a specific laminate, however, is assumed to have the same fiber volume fraction as that of the laminate, and the same thickness which is equal to one fourth of the laminate thickness. The material and fabric geometric parameters given in Table 11 were used as input data. In the table the yarn diameter d was determined using a fiber mass density of ρ_f=2.54g/cm3 and a fiber packing density (fiber volume content in the yarn) of 0.907 /27/. However, as only the planar coordinates of the yarns in the RVE are employed, the fiber packing density and hence the yarn diameter did not have any significant effect on the simulation. The predicted results are summarised in Table 12. Compared with Table 11, it is clearly seen that correlation between the predicted and the measured data is reasonably good.

4.3 Case Study

Various material and geometric parameters involved can affect the mechanical performance of a knitted fabric reinforced composite laminate, including the fabric lay-up configuration, the overall fiber volume fraction, the knitting parameters (i.e., stitch density), and the matrix ultimate strength. As the influence of fabric geometric parameters and the constituent properties on the strength of a single layer knitted fabric reinforced composite lamina has been investigated extensively in the previous Sections, only the effect of fabric lay-up configurations on the laminate strength is considered herein. Fig. 24 indicates the first ply and the last ply failure strengths of $[0/\theta/-\theta/0]$ laminate subjected to a uniaxial load in the 0-direction varied with the plied angle θ from 0 to 90 degree, whereas Fig. 25 graphs similar variation of $[\theta/-\theta/-\theta/\theta]$ laminates. From the figures, we can see that neither type of laminates has a significant difference in the first and last ply failure strengths. For the laminate type, $[0/\theta/-\theta/0]$, the ultimate failure strength gradually reduces as the ply angle, θ, increases from 0 to 90 degree, and attains a minimum value as θ=90°. On the other hand, the ultimate failure strength of laminate type, $[\theta/-\theta/-\theta/\theta]$, already attains a minimum value at about θ=60°.

Finally, investigation of the load carrying capacity of several laminates subjected to biaxial loads is performed, as plotted in Figure 26. Amongst the investigated laminates, [0/0/0/0], [0/45/-45/0],and [0/90/-90/0], the load carrying capacity of the [0/45/-

Table 12

Predicted tensile properties of plain knitted E-glass fiber fabric reinforced epoxy composite laminates. Parameters used are: E^f=74GPa, E^m=2.32GPa, ν^f=0.23, ν^m=0.42, E_T^m =527MPa, σ_T^m =27MPa, σ_u^f =1933MPa, σ_u^m =39.2MPa, d=0.0586cm, C=3.46loop/cm, and W=3.86loop/cm.

Laminate lay-up	V_f	Prediction in load direction			Load direction
		Modulus (GPa)	Strength (MPa)		
			1st ply failure	Last ply failure	
[0/0/0/0]	0.226	5.96	88.8	88.8	Wale (0)
[90/90/90/90]	0.235	4.11	51.0	51.0	Course (90)
[0/90/90/0]	0.210	4.86	67.2	69.8	Wale (0)
[0/45/-45/0]	0.217	5.42	71.2	79.8	Wale (0)

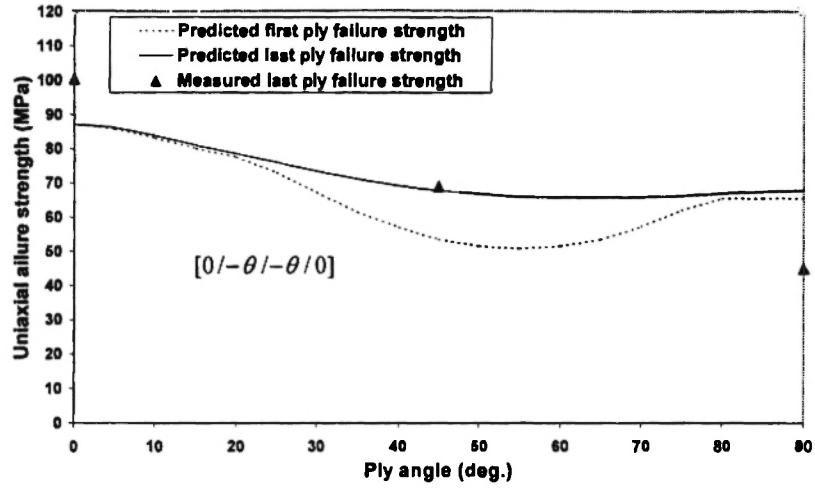

Fig. 24: First ply and last ply failure strengths of knitted fabric laminates, [0/θ/-θ/0], varied with ply angle θ. The parameters used, except for V_f=0.21, were taken from Table 11.

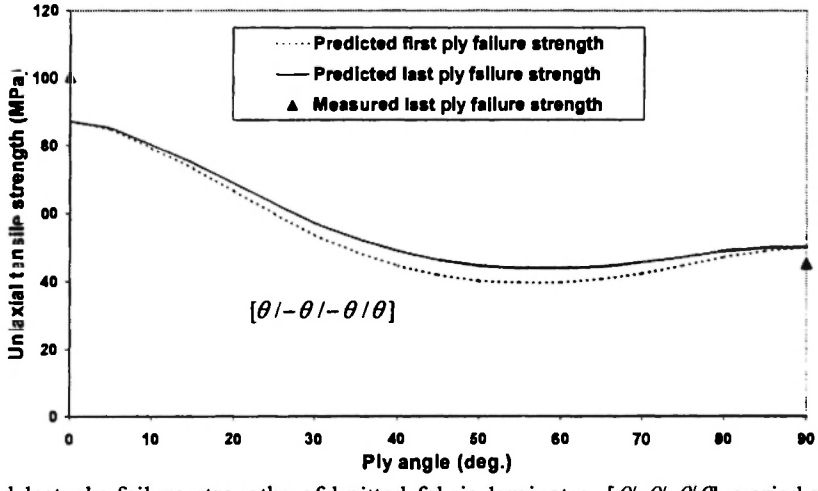

Fig. 25: First ply and last ply failure strengths of knitted fabric laminates, [θ/-θ/-θ/θ], varied with ply angle θ. The parameters used, except for V_f=0.21, were taken from Table 11.

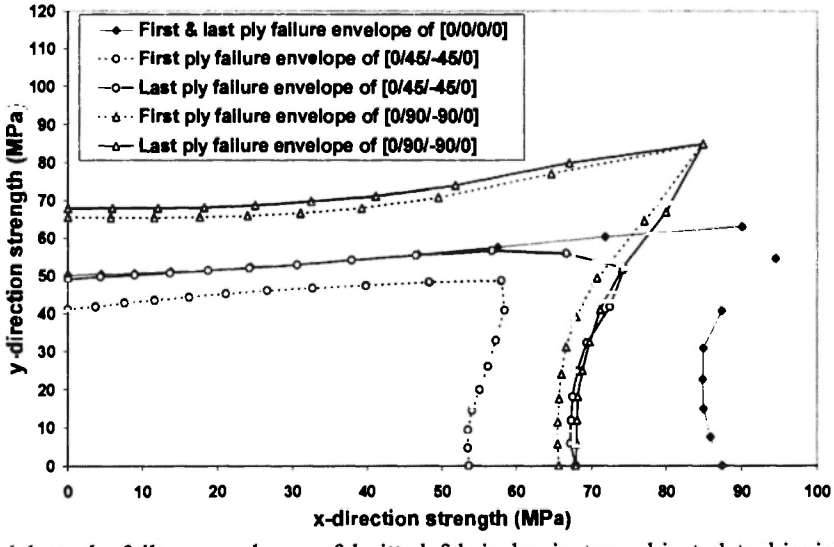

Fig. 26: First ply and last ply failure envelopes of knitted fabric laminates subjected to biaxial tensile loads. The parameters used, except for V_f=0.21, were taken from Table 11.

45/0] laminate is grossly the least, whereas the [0/90/-90/0] laminate is able to sustain generally higher load combination than the [0/0/0/0] laminate, as long as the load value in the x (wale) direction is not significantly higher than that in the y (course) direction. Otherwise, i.e., if there is a dominant load in the wale direction, the [0/0/0/0] laminate should be employed. Further, only for the [0/45/-45/0] laminate, the first ply failure envelope is distinctly different from the last ply failure envelope, whereas the two other laminates, i.e., the [0/0/0/0] and [0/90/-90/0] laminates, exhibit nearly the same first and last ply failure envelopes.

5. CONCLUDING REMARKS

The structure-property of a knitted fabric reinforced composite can be simulated micromechanically, as long as its constituent properties and the fabric geometric parameters are all known. Two typical types of knitted fabric reinforced composite materials, i.e., thermoset and elastomer matrix based composites, have been investigated, and reviewed and summarized in this series of papers. Various material and geometric variables can influence the composite properties. However, the most dominant influencing variables are the properties of the matrix material used, especially on the composite strength. It has been found that the failure of a knitted fabric composite is essentially initiated from the matrix failure, no matter what kind of load is applied to the composite. This is different from a unidirectional or multidirectional tape laminate, the failure of which can also be caused by the fiber fracture if loaded in the fiber direction.

The simulation work presented in this paper is based on type I (Fig. 21 of Ref. /1/) weft knitted fabric structures. However, application to the composites reinforced with other types of weft or warp knitted fabrics is straightforward. The main issue involved is how to identify the geometry of a RVE of such a composite, i.e., to identify the fabric geometry.

Investigation of thermoplastic matrix based knitted fabric composites is slightly different. This kind of composites is generally fabricated by melting the matrix materials at relatively high temperatures. Hence, from a simulation point of view, the most significant feature of thermoplastic matrix composites, relative to thermoset matrix composites, is that the resulting thermal residual stresses must be taken into account in nonlinear and failure analysis. Due to mismatch between the coefficients of thermal expansion of the fibers and the matrix, thermal residual stresses are generated in the constituent fibers and matrix. Whereas these stresses essentially have no effect on the composite stiffness, they do have an influence on the composite load carrying capacity. Proper and accurate incorporation of these stresses into the bridging model analysis is possible /28,29/.

Additional future work may concentrate on two issues. The first involves further development of the micromechanics model itself. The currently used bridging matrix has not considered the effect of debonding of fiber/matrix interface and other fabrication defects on the mechanical properties of composites. The damage evolution has not been taken into account either. To incorporate all these effects, the bridging matrix should be modified accordingly and might have different forms at different load levels. The second issue is related to peculiar features of knitted fabric composites. It has been seen that the modeling work presented in this paper did not consider any effect of stress concentration. Because of looped structure, the stress level in some part of the fabric yarn must be higher than the stress level in the other part. This difference should not be merely due to different yarn orientation, but should also have contained the contribution of curvature induced extra stresses. The modeling work presented in this series of papers, however, could not identify these extra stresses. Since a perfect bonding assumption was used, the predicted failure model can only be either the fiber fracture or the matrix failure. In practice, we have also observed the evidence of fiber/matrix interface debonding. Although such a debonding can be attributed to the crack initiation in the matrix material, incorporation of damage evolution until the failure of both constituent materials may be more pertinent in the case of knitted fabric composites. Furthermore, the modeling work conducted so far is only related to static loading situation. Fatigue and the dynamic load response of knitted fabric composites have not been tackled at all. Investigation of these dynamic properties will be another topic for future research.

REFERENCES

1. Huang, Z. M. and Ramakrishna, S., Modeling Mechanical Properties of Knitted Fabric Composites-Part I: Overview and Geometric Description, *Science & Engineering of Composite Materials*, Vol. 10, No. 3, pp. 163-188.
2. Huang, Z. M. and Ramakrishna, S., Modeling Mechanical Properties of Knitted Fabric Composites-Part II: Theoretical Description, *Science & Engineering of Composite Materials*, Vol. 10, No. 3, pp. 189-211.
3. Rudd, C. D., Owen, M. J., & Middleton, V., 1990, Mechanical Properties of Weft Knit Glass Fiber/Polyester Laminates, *Comp. Sci. & Tech.*, Vol. 39, pp. 261-277.
4. Ramakrishna, S., 1997, Characterization and Modeling of the Tensile Properties of Plain Weft-Knit Fabric-Reinforced Composites, *Comp. Sci. & Tech.*, Vol. 57, pp. 1-22.
5. Ramakrishna, S., Huang, Z. M., Teoh, S. H., Tay, A. A. O., and Chew, C. L., 2000, Application of Leaf and Glaskin's Model for Estimating the 3D Elastic Properties of Knitted Fabric Reinforced Composites, *J. Text. Inst.*, Vol. 91 Part 1, No. 1, pp. 1-19.
6. Huang, Z. M., Ramakrishna, S., and Tay, A. A. O., 1999, A Micromechanical Approach to the Tensile Strength of a Knitted Fabric Composite, *J. of Comp. Mater.*, Vol. 33, No. 19, pp. 1758-1791.
7. Huang, Z. M., Ramakrishna, S., and Tay, A. A. O., 2000, Unified Micromechanical Model for Estimating Elastic, Elasto-Plastic, and Strength Behaviors of Knitted Fabric Reinforced Composites, *J. Reinf. Plast. & Comp.*, Vol. 19, No. 8, pp. 642-656.
8. Huang, Z. M. and Ramakrishna, S., 2000, Micromechanical modeling approaches for the stiffness and strength of knitted fabric composites: A review & comparative study, *Composite A*, Vol. 31, No. 5, pp. 479-501.
9. Huang, Z. M., Ramakrishna, S. and Leong, K. H., 2002, Modeling the Tensile Behavior of Milano Rib Knit Fabric Composites, *J. Reinf. Plastics & Comp*, Vol. 21, No. 12, pp. 1123-1146.
10. Leong, K. H., Falzon, P. J., Bannister, M. K. and Herszberg, I., 1998, An Investigation of the Mechanical Performance of Weft-Knitted Milano Rib Glass/Epoxy Composites, *Comp. Sci. & Tech.*, Vol. 58, pp. 239-251.
11. Ramakrishna, S., Tang, Z. G., and Teoh, S. H., 1997, Development of a Flexible Composite Material, Advanced Composite Letters, Vol. 6, No. 1, pp. 5-8.
12. Pipkin, A. C., 1974, Finite Deformations of Ideal Fiber-Reinforced Composites, in *Machanics of Composite Materials*, G. P. Sendeckyj ed., Academic Press, New York, pp. 251-308.
13. Adkins, J. E. & Rivlin, R. S., 1955, Large Elastic Deformation of Isotropic Materials *X*: Reinforcements by Inextensible cords, *Phil. Trans. Royal Soc. London*, (A), Vol. 248, pp. 201-223.
14. Pinkin, A. C. & Roger, T. G., 1971, Plane Deformation of Incompressible Fiber-Reinforced Materials, *J. Appl. Mech.*, Vol. 38, pp. 634-640.
15. Spencer, A. J. M., 1972, Deformation of Fiber Reinforced Materials, Clarendon Press, Oxford.
16. Hahn, H. T., 1973, Nonlinear Behavior of Laminated Composites, *J. Comp. Materials*, Vol. 7, pp. 257-271.
17. Hahn, H. T. & Tsai, S. W., 1973, Nonlinear Elastic Behavior of Unidirectional Composite Laminae, *J. Comp. Materials*, Vol. 7, pp. 102-118.
18. Jones, R. S. & Morgan, H. S., 1977, Analysis of Nonlinear Stress-Strain Behavior of Fiber-Reinforced Composite Materials, *AIAA J.*, Vol. 15, pp. 1669-1676.
19. Luo, S. Y. & Chou, T. W., 1988, Finite Deformation and Nonlinear Elastic Behavior of Flexible Composites, *J. Appl. Mech.*, Vol. 55, pp. 149-155.
20. Luo, S. Y. & Chou, T. W., 1990, Finite Deformation of Flexible Composites, *Proc. Royal Soc. London*, (A), Vol. 429, pp. 569-586, pp. 149-155.
21. Chou, T. W., 1992, Microstructural Design of Fiber Composites, Ch. 9, Nonlinear Elastic Finite Deformation of Flexible Composites, Cambridge University Press, Cambridge, pp. 475-525.
22. Huang, Z. M., Ramakrishna, S., Dinner, H. P., and Tay, A. A. O., 1999, Characterization of a Knitted Fabric Reinforced Elastomer Composite, *J. Reinf.*

Plast. & Comp., Vol. 18, No. 2, pp. 118-137.

23. Huang, Z. M., Ramakrishna, S., and Tay, A. A. O., 2000, Modelling of Stress-Strain Behavior of a Knitted Fabric Reinforced Elastomer Composite, *Comp. Sci. & Tech.*, Vol. 60, No. 5, pp. 671-691.
24. Hinton, M. J. and Soden, P. D., 1998, Predicting Failure in Composite Laminates: The Background to the Exercise, *Comp. Sci. & Tech.*, Vol. 58, pp. 1001-1010.
25. Huang, Z. M., 2001, Effect of Matrix Plasticity on Ultimate Strength of Composite Laminates, *J. of Reinforced Plastics & Composites*, Vol. 20, No. 4, pp. 304-320.
26. Huang, Z. M., Zhang, Y.-Z., and Ramakrishna, S., 2001, Modeling Progressive Failure Process of Multilayer Knitted Fabric Reinforced Composite Laminates, *Comp. Sci. & Tech.*, Vol. 61, No. 14, pp. 2033-2046.
27. Ruan, X. P. & Chou, T. W., 1996, Experimental and Theoretical Studies of the Elastic Behavior of Knitted-Fabric Composites, *Comp. Sci. & Tech.*, Vol. 56, pp. 1391-1403.
28. Huang, Z. M., 2000, Strength Formulae of Unidirectional Composites Including Thermal Residual Stresses, *Materials Letters*, Vol. 43, No. 1-2, pp. 36-42.
29. Huang, Z. M., 2001, Modeling Strength of Multidirectional Laminates under Thermo-Mechanical Loads, *J. Comp. Mater.*, Vol. 35, No. 4, pp. 281-315.